

ORIGINAL RESEARCH

Open Access



# Human biodistribution and radiation dosimetry of the 5-HT<sub>2A</sub> receptor agonist Cimbi-36 labeled with carbon-11 in two positions

Annette Johansen<sup>1,2</sup>, Søren Holm<sup>3</sup>, Bente Dall<sup>3</sup>, Sune Keller<sup>3</sup>, Jesper L. Kristensen<sup>4</sup>, Gitte M. Knudsen<sup>1,2\*</sup>  and Hanne D. Hansen<sup>1</sup>

## Abstract

**Background:** Cimbi-36 can be <sup>11</sup>C-labeled to form an agonist radioligand used for positron emission tomography (PET) imaging of the 5-HT<sub>2A</sub> receptor in the brain. In its non-labeled form (25B-NBOMe), it is used as a recreational drug that can lead to severe adverse effects, in some cases, with fatal outcome. We investigated human biodistribution and radiation dosimetry of the radioligand with two different radiolabeling positions. Seven healthy volunteers underwent dynamic 120-min whole-body PET scans (injection of 581 ± 16 MBq, *n* = 5 for <sup>11</sup>C-Cimbi-36; 593 ± 14 MBq, *n* = 2 for <sup>11</sup>C-Cimbi-36\_5). Time-integrated activity coefficients (TIACs) from time-activity curves (TACs) of selected organs were used as input into the OLINDA/EXM software to obtain dosimetry information for both <sup>11</sup>C-labeling positions of Cimbi-36.

**Results:** The effective dose was only slightly higher for <sup>11</sup>C-Cimbi-36 (5.5 μSv/MBq) than for <sup>11</sup>C-Cimbi-36\_5 (5.3 μSv/MBq). Standard uptake value (SUV) curves showed higher uptake of <sup>11</sup>C-Cimbi-36 in the pancreas, small intestines, liver, kidney, gallbladder, and urinary bladder compared with <sup>11</sup>C-Cimbi-36\_5, reflecting differences in radiometabolism for the two radioligands. Variability in uptake in excretory organs for <sup>11</sup>C-Cimbi-36 points to inter-individual differences with regard to metabolic rate and route. Surprisingly, moderate uptake was found in brown adipose tissue (BAT) in four subjects, possibly representing specific 5-HT<sub>2A/2C</sub> receptor binding.

**Conclusion:** The low effective dose of 5.5 μSv/MBq allows for the injection of up to 1.8 GBq for healthy volunteers per study (equivalent to 3 scans if injecting 600 MBq) and still stay below the international guidelines of 10 mSv, making <sup>11</sup>C-Cimbi-36 eligible for studies involving a series of PET scans in a single subject. The biodistribution of Cimbi-36 (and its metabolites) may also help to shed light on the toxic effects of 25B-NBOMe when used in pharmacological doses in recreational settings.

**Keywords:** <sup>11</sup>C-Cimbi-36, 25B-NBOMe, 5-HT<sub>2A</sub> receptor, Biodistribution, Pharmacology, Pharmacokinetics, Positron emission tomography, Radiation dosimetry

\* Correspondence: [gmk@nru.dk](mailto:gmk@nru.dk)

<sup>1</sup>Neurobiology Research Unit and Center for Integrated Molecular Brain Imaging, Rigshospitalet, Building 6931, Blegdamsvej 9, DK-2100 Copenhagen, Denmark

<sup>2</sup>Faculty of Health and Medical Sciences, University of Copenhagen, Copenhagen, Denmark

Full list of author information is available at the end of the article

## Introduction

Cimbi-36 can be labeled with carbon-11 to form a positron emission tomography (PET) radioligand for imaging of serotonin 2A receptor (5-HT<sub>2A</sub>R) agonist binding in the human brain [1]. 5-HT<sub>2A</sub>Rs are widely distributed in the cerebral cortex [2] and has been linked to neuropsychiatric disorders such as depression [3, 4]. Further, many antipsychotic medications act as antagonist or inverse agonists on the 5-HT<sub>2A</sub>R [5], while psychedelic effects are shown to correlate with 5-HT<sub>2A</sub>R occupancy following administration of the classical hallucinogen, psilocybin [6]. The Cimbi-36 molecule (*N*-(2-methoxybenzyl)-2,5-dimethoxy-4-bromophenethylamine) itself acts as an agonist on the 5-HT<sub>2A</sub>R and is used in pharmacological doses as a recreational drug, known as 25B-NBOMe, belonging to the class of new psychoactive substances [7].

<sup>11</sup>C-labeled Cimbi-36 is presently the only agonist radioligand available for imaging the 5-HT<sub>2A</sub>R [8], and it is known that agonists and antagonists interact in different modes with the receptor [9]. Cimbi-36 has been widely characterized in terms of *in vitro* receptor binding [10], preclinical evaluation of safety, pharmacological effects, and functionality as a PET tracer [11, 12]. As of yet, no studies on human biodistribution or radiation dosimetry of <sup>11</sup>C-labeled Cimbi-36 have been conducted. Extrapolations from pig and rat dosimetry are available [11], but differences across species cannot be predicted [13].

Metabolism of Cimbi-36 has been of interest, not just because of its use in neuroreceptor imaging, but also due to illicit use as a recreational drug [14]. This, in turn, has shed light on the relationship between the <sup>11</sup>C-labeling position and radiolabeled metabolites and their effects on binding estimates [15]. In this study, we not only compare human dosimetry estimates of two <sup>11</sup>C-labeling positions of the PET radioligand Cimbi-36 (<sup>11</sup>C-Cimbi-36 (*N*-(2-[<sup>11</sup>C-OCH<sub>3</sub>]-methoxybenzyl)-2,5-dimethoxy-4-bromophenethylamine) vs <sup>11</sup>C-Cimbi-36\_5 (*N*-(2-methoxybenzyl)-2-methoxy-5-[<sup>11</sup>C-OCH<sub>3</sub>]-methoxy-4-bromophenethylamine) but also provide new information on biodistribution and pharmacokinetics of the controlled substance, 25B-NBOMe.

## Materials and methods

### Study design

The study was approved by the Ethics Committee for the Capital Region of Denmark (protocol no. H-15001910) and the Danish Health and Medicine Authority (EudraCT no. 2015-004256-21). The study was registered as a clinical trial (NCT02629003) at [ClinicalTrials.gov](https://clinicaltrials.gov) and was performed in accordance with the recommendation for Good Clinical Practice. Study participants were recruited through online advertisement and all participants gave written informed consent after a detailed explanation of

the study. Whole-body distribution and radiation dosimetry of <sup>11</sup>C-Cimbi-36 and <sup>11</sup>C-Cimbi-36\_5 were investigated with PET/CT imaging. Eight healthy volunteers (mean age 20.6 ± 2.8 years, 5 females) were included in the study. The radiotracers were produced as previously described [14].

### Whole-body PET/CT acquisition

Scanning was performed with a Siemens Biograph mCT PET/CT system that was normalized daily using a Ge-68 cylinder phantom and cross-calibrated to gamma counter and radionuclide calibrator in a biweekly routine process using F-18. Prior to intravenous injection of the radiotracer (aimed at 600 MBq) in the antecubital vein, the subjects underwent a low-dose CT scan for subsequent anatomical localization. The 120-min PET scan started at the time of injection with an initial 3-min list mode acquisition over the heart (not presented here), followed by (up to) 16 whole-body scan passes with increasing scan time. Each scan pass covered a total of 198 cm in 15 bed positions (axial field of view 21.6 cm, overlap 9.0 cm). For the first 4 passes, scan time per bed position was 15 s (5 s over the legs). This was increased for pass 5–8 to 30 s (10 s) and for the final 8 passes to 60 s (20 s). PET reconstruction was done using 3 iterations and 21 subsets OSEM3D with TOF and Siemens mCT standard scatter correction, random correction, and low-dose CT-based attenuation correction. A 5-mm FWHM Gaussian post-reconstruction filter was applied.

Venous blood was drawn from the opposite antecubital vein for whole blood (WB) radioactivity measurement.

### Estimation of whole-body distribution and radiation dose

For each subject, scans were analyzed using Mirada RTx (Mirada Medical, Oxford, UK) as previously described [16, 17], but with some modifications, for the following organs: thyroid, heart wall, liver, spleen, kidney, bone, bone marrow (the central part of the L4-L5 vertebrae was used as a surrogate), stomach wall and contents, subcutaneous fat, and periclavicular brown adipose tissue (BAT), 2–3 VOIs (volume ranging from 7 mL (thyroid gland) to 63 mL (liver)) were drawn based on the PET image and cross-checked with the anatomical CT image. For the following organs, a single VOI was placed encompassing most of the organ based on the CT image and also guided by PET images; brain, lungs, gallbladder, pancreas, proximal part of the small intestines, and large intestines. To account for the change in volume of the urinary bladder during the scan, the bladder (contents) region was drawn based on the PET images for subjects scanned with <sup>11</sup>C-Cimbi-36. This was not possible for images of <sup>11</sup>C-Cimbi-36\_5, as the activity could not be discerned from surrounding tissue. For each time point, decay-uncorrected activity concentration (kBq/

mL) and standard uptake values (SUVs; g/mL, by definition decay-corrected) were extracted. Cumulated activity for each organ was estimated as the area under the curve (AUC; kBq/mL  $\times$  h (kBq per mL times h)) for each subject using the trapezoid method. Although of minor importance since the integration already covers six half-lives of the tracer, extrapolation from the last time point to infinity was done by adding  $A_{120 \text{ min}}/k$  ( $k$  being the decay constant for carbon-11), thus assuming simple physical decay. These values were subsequently normalized by dividing by injected activity and then multiplied by standard organ masses of the OLINDA male or female adult phantom [18], thereby estimating the time-integrated activity coefficients (TIAC, formerly known as *residence time*; unit *h*) for each organ. Individual TIACs were scaled by the ratio of the individual subject's body mass to standard phantom body mass, then averaged across subjects ( $n = 5$  or  $n = 2$ ) and entered into the OLINDA/EXM 2.0 software to obtain estimates of absorbed and effective doses with tissue weighting factors according to ICRP 103 [19]. With this method, we use the principle for extrapolation from animal data (known as the % injected dose/g method) [20] to human data, except that we extrapolate from a small sample of humans to the general population.

Urinary bladder contents data were incorporated using the bladder voiding model in OLINDA as a practical way to estimate absorbed dose to the bladder wall. For each subject scanned with  $^{11}\text{C}$ -Cimbi-36, cumulated decay-corrected activity (in kBq) was plotted over time and fitted using a one phase association equation in GraphPad Prism (GraphPad Prism version 8.0.0 for MacOS, GraphPad Software, San Diego, CA, USA, [www.graphpad.com](http://www.graphpad.com)). The results of these fits were inserted into the Olinda software, and the returned urinary TIACs were averaged across subjects. A bladder voiding interval of 2 h was used, which essentially means that activity is accumulated and excreted only once, since less than 2% of the activity is left after 2 h. TIACs of remainder tissue were calculated as the total number of decays minus the sum of the organ-specific values. For  $^{11}\text{C}$ -Cimbi-36\_5 we used post-scan cumulated urine activity to yield excretory fraction estimate.

## Results

### Dosimetry estimation

Five participants (three females, two males) completed  $^{11}\text{C}$ -Cimbi-36 PET/CT scans (injection of  $581 \pm 16$  MBq; specific activity at the time of injection was  $665 \pm 240$  GBq/ $\mu\text{mole}$ ;  $0.37 \pm 0.15$   $\mu\text{g}$ ) according to protocol. Two participants (two females) completed the  $^{11}\text{C}$ -Cimbi-36\_5 PET/CT scan (injection of 583–603 MBq;

specific activity at the time of injection was 365–583 GBq/ $\mu\text{mole}$ ; 0.38–0.63  $\mu\text{g}$ ) according to protocol. We originally planned to include 10 subjects, but 1 female participant did not complete the scan as the production of radiotracer failed. We refrained from completing the last two planned  $^{11}\text{C}$ -Cimbi-36\_5 scans, as the decision to use the  $^{11}\text{C}$ -Cimbi-36 labeling position for future 5-HT<sub>2A</sub>R imaging studies was made before the completion of this study [15], regardless of the dosimetry outcome. Thus, for ethical reasons the study was halted. No adverse events occurred.

Whole-body PET/CT images 40 min into the scan are shown for both radioligands in Fig. 1. Data from the organ VOIs (see Additional file 1: Supplementary Table S1 for the individual TIACs) were quantified and processed using the Olinda software, yielding absorbed and effective doses, as seen in Table 1.

The effective doses were 5.5  $\mu\text{Sv}/\text{MBq}$  and 5.3 for  $^{11}\text{C}$ -Cimbi-36 and  $^{11}\text{C}$ -Cimbi-36\_5, respectively. For  $^{11}\text{C}$ -Cimbi-36, the organs with the highest contributions to effective dose were the lungs, urinary bladder, liver, stomach wall, and red marrow, all contributing more than 0.50  $\mu\text{Sv}/\text{MBq}$ . For most organs,  $^{11}\text{C}$ -Cimbi-36\_5 yielded lower absorbed doses, with the highest contribution to effective dose ( $>0.50$   $\mu\text{Sv}/\text{MBq}$ ) found again in the lungs, stomach wall, liver, and red marrow. The most noticeable difference between the radioligands was found in the urinary bladder (ratio of 5).

No discernible radioactivity uptake was seen in the reproductive organs (uterus, ovaries, testes) for  $^{11}\text{C}$ -Cimbi-36 (three females, two males) or  $^{11}\text{C}$ -Cimbi-36\_5 (two females). Thus, the absorbed and effective doses are based on radiation from neighboring organs and the remainder activity. In the case of  $^{11}\text{C}$ -Cimbi-36\_5, radiation to the testes is based on extrapolation to the male phantom in Olinda (Table 1).

### Biodistribution

SUV curves for both radiotracers (including their respective radiolabeled metabolites) are shown in Fig. 2 for selected organs, and individual subjects' SUV curves for whole blood and excretory organs in Fig. 3. For the lungs, thyroid, and spleen, the curves are virtually identical for the two radioligand-labeling positions, with the spleen showing the highest initial uptake ( $>12$  g/mL). The pancreas, small intestines, liver, kidney, gallbladder, and urinary bladder all have a higher uptake of  $^{11}\text{C}$ -Cimbi-36 compared with  $^{11}\text{C}$ -Cimbi-36\_5. This difference emerges after varying time intervals for the organs; liver (app. 15 min), kidney (20 min), gallbladder (60 min), and urinary bladder (10 min), and for the gallbladder and urinary bladder, it continues to increase throughout the scan.

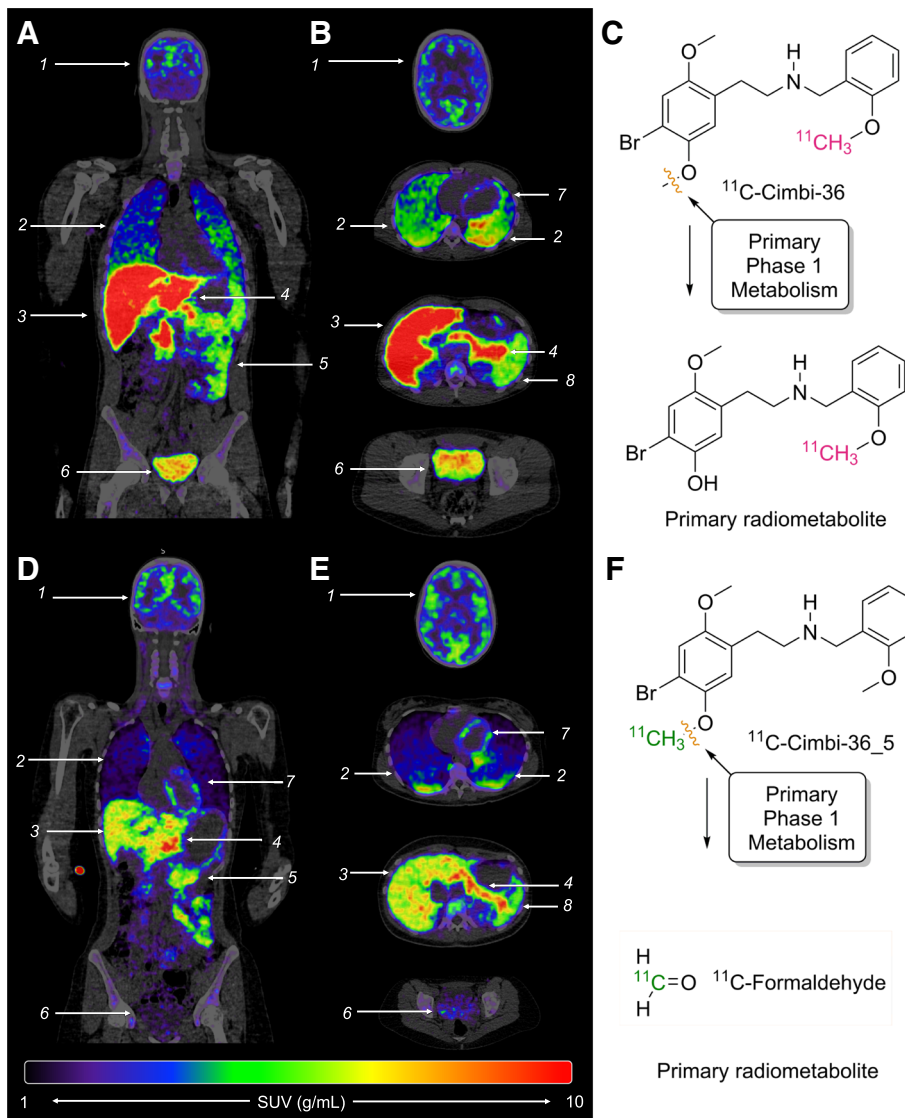


**Fig. 1** Coronal and horizontal PET/CT fused images of  $^{11}\text{C}$ -Cimbi-36 (**a, b**) and  $^{11}\text{C}$ -Cimbi-36\_5 (**d, e**) 40 min into the scan. Brain (1), lungs (2), liver (3), pancreas (4), small intestines (5), urinary bladder (6), heart wall (7), spleen (8). Primary phase 1 metabolic route resulting in different radiometabolites for  $^{11}\text{C}$ -Cimbi-36 (**c**) and  $^{11}\text{C}$ -Cimbi-36\_5 (**f**)

Moderate uptake in four of the seven participants was, surprisingly, found in what we believe to be brown adipose tissue (Fig. 4a). Localized on the side of the neck and close to the clavicular bone, we found fatty tissue (verified through visual inspection [21] and corroborated by Hounsfield unit values) with clearly detectable uptake. The subjects with these findings were all female (mean age 23 years, range 19–25; mean body mass index 21.9, range 18.8–27.9), two had been scanned with  $^{11}\text{C}$ -Cimbi-36 and two with  $^{11}\text{C}$ -Cimbi-36\_5. The SUV curves in BAT closely resembles the whole brain SUVs, and in order to distinguish the uptake from non-specific binding to fatty tissue in general, we compared them with SUVs derived from a VOI in subcutaneous fat of the abdomen (Fig. 4b).

## Discussion

### Dosimetry estimates

In this study, we evaluated human radiation dosimetry for the  $^{11}\text{C}$ -labeled 5-HT<sub>2A</sub>R agonist PET radioligand, Cimbi-36, using two different  $^{11}\text{C}$ -labeling positions. Effective dose for  $^{11}\text{C}$ -Cimbi-36, the labeling position of choice for neuroimaging [15], was 5.5  $\mu\text{Sv}/\text{MBq}$ , resulting in a radiation dose of 3.3 mSv for a PET scan following injection of 600 MBq and allows for injection of 1.8 GBq per study in order to stay below 10 mSv, which is the recommended limit for studies involving healthy volunteers, that provide *intermediate* to *moderate* benefits to society [22].

$^{11}\text{C}$ -Cimbi-36 is a radioligand developed for brain imaging, and thus magnetic resonance imaging is often

**Table 1** Organ absorbed doses and contributions to effective doses for  $^{11}\text{C}$ -Cimbi-36 and  $^{11}\text{C}$ -Cimbi-36\_5

Target organ	Absorbed dose ( $\mu\text{Gy}/\text{MBq}$ )		Contributions to effective dose ( $\mu\text{Sv}/\text{MBq}$ )	
	$^{11}\text{C}$ -Cimbi-36	$^{11}\text{C}$ -Cimbi-36_5	$^{11}\text{C}$ -Cimbi-36	$^{11}\text{C}$ -Cimbi-36_5
Adrenals	5.83	5.52	0.05	0.05
Brain	6.12	6.72	0.06	0.07
Breasts	2.38	2.42	0.29	0.29
Esophagus	3.54	3.50	0.14	0.14
Eyes	2.19	2.32	0.00	0.00
Gallbladder wall	5.85	4.88	0.05	0.05
Left colon	5.24	5.70	0.25	0.28
Small intestine	5.55	4.91	0.05	0.05
Stomach wall	5.46	7.56	0.66	0.91
Right colon	3.23	3.15	0.16	0.15
Rectum	2.99	2.57	0.07	0.06
Heart wall	10.70	9.84	0.10	0.09
Kidneys	11.80	10.50	0.11	0.10
Liver	15.70	13.20	0.63	0.53
Lungs	8.61	8.31	1.03	1.00
Ovaries	3.14	2.91	0.13	0.12
Pancreas	13.30	11.60	0.12	0.11
Prostate	2.67	2.29	0.01	0.01
Salivary glands	2.36	2.48	0.02	0.02
Red marrow	4.19	4.33	0.50	0.52
Osteogenic cells	3.37	3.72	0.03	0.04
Spleen	18.40	17.90	0.17	0.17
Testes	1.89	1.87	0.08	0.07
Thymus	3.20	3.21	0.03	0.03
Thyroid	6.37	6.52	0.26	0.26
Urinary bladder wall	12.40	2.40	0.50	0.10
Uterus	3.51	2.85	0.02	0.01
Effective dose			5.5	5.3

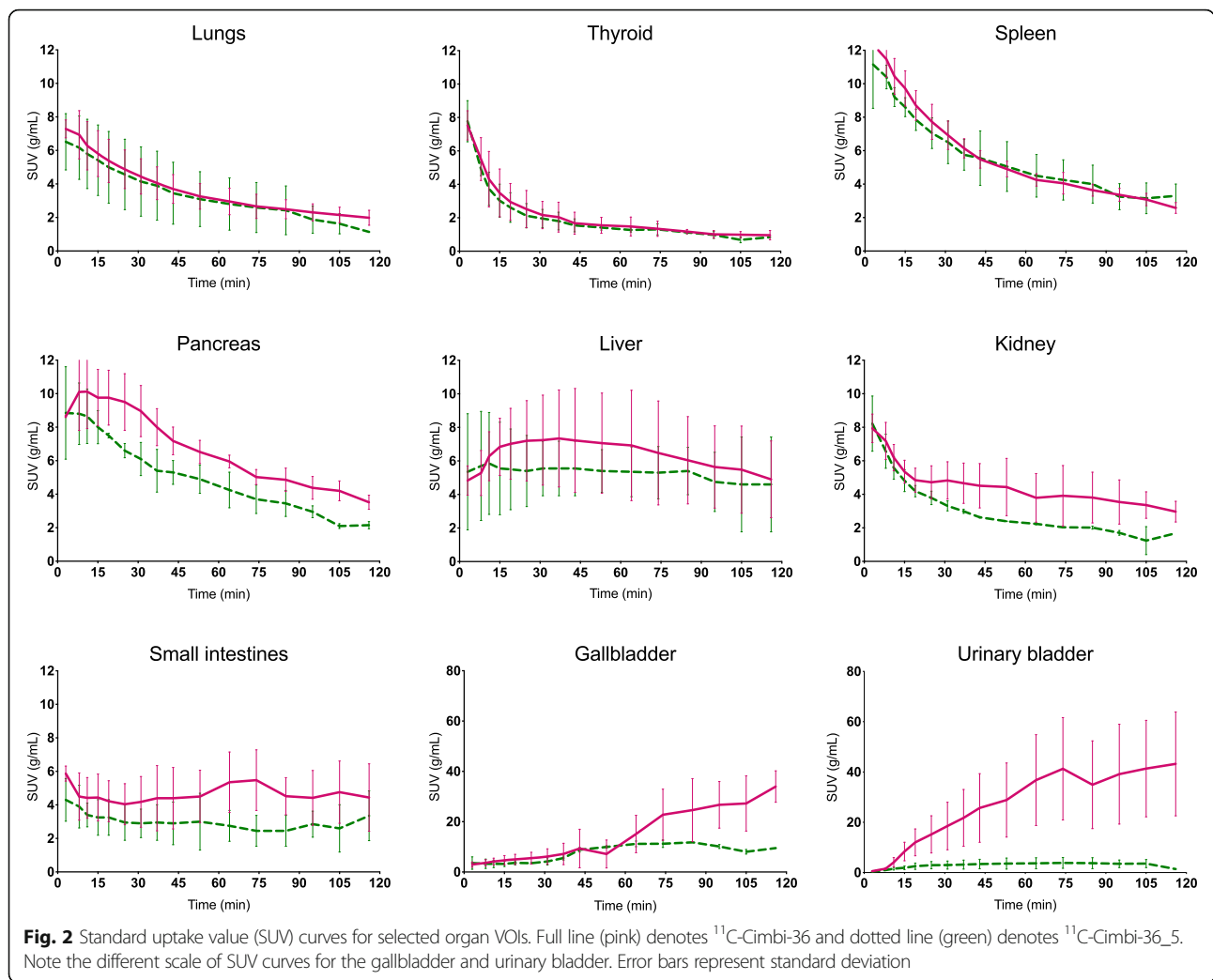
used for anatomical purpose, yielding no additional radioactive exposure. However, a low-dose brain-only CT for attenuation correction can be performed at a fraction of the PET effective dose.

Because of the short half-life of carbon-11 (20.4 min), organs with high perfusion tend to get the highest absorbed doses of radiation from  $^{11}\text{C}$ -labeled radioligands, but also excretory organs such as the liver, kidney, gallbladder, and urinary bladder get high exposure [23]. Indeed, this is also true for  $^{11}\text{C}$ -Cimbi-36, as the liver, kidneys, and urinary bladder are among the five organs with highest absorbed doses. This reflects the relatively fast metabolism seen for Cimbi-36 [1, 15].

The effective dose for the alternative labeling position,  $^{11}\text{C}$ -Cimbi-36\_5, was only slightly lower; 5.3  $\mu\text{Sv}/\text{MBq}$  (equivalent to a radiation dose of 3.2 mSv if injecting

600 MBq), with the difference being most pronounced for the urinary bladder, i.e., a fivefold reduction in absorbed dose. Despite the small sample size, the generally lower uptake for  $^{11}\text{C}$ -Cimbi-36\_5, including in the urinary bladder, can be attributed to the higher level of radioactivity in the form of small diffusible substances ( $^{11}\text{C}$ -formaldehyde,  $^{11}\text{C}$ -formic acid), and possibly also volatile ( $^{11}\text{C}$ - $\text{CO}_2$ ) substances, comprised in the M1 radiometabolite fraction (Fig. 1) [15].

The difference in effective dose between the two  $^{11}\text{C}$ -labelings of Cimbi-36 is within the limitations of the method and inter-individual variability. Thus, even the relatively fast metabolism of parent tracers (resulting in radiometabolites with different physical properties) does not affect dosimetry outcomes noticeably. This attests to the notion that dosimetry of  $^{11}\text{C}$ -



labeled radioligands is mostly dependent on the initial blood perfusion phase.

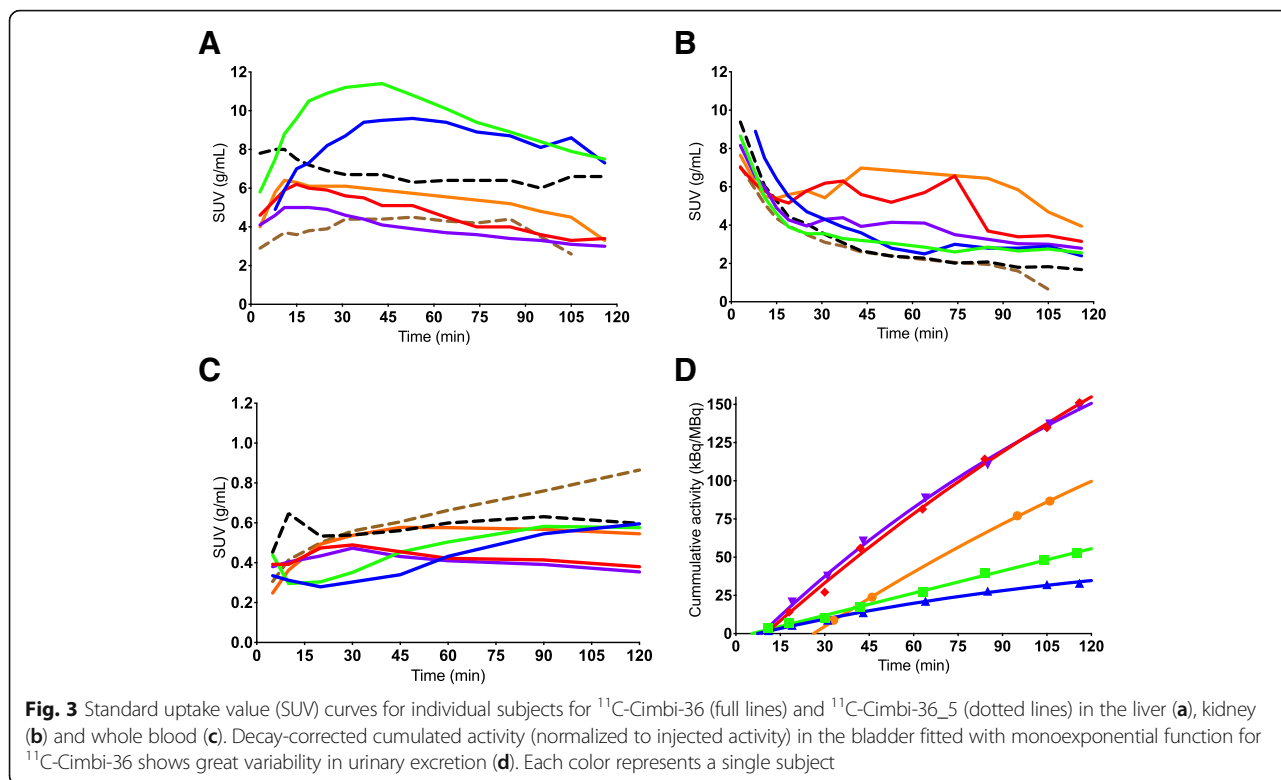
The effective doses of both radioligands are in line with other  $^{11}\text{C}$ -labeled PET tracers; range 3.0–7.8  $\mu\text{Sv}/\text{MBq}$ , with the exception of one ( $^{11}\text{C}$ -WAY-100635; 14.1  $\mu\text{Sv}/\text{MBq}$ ) [13, 23]. The estimated effective dose for  $^{11}\text{C}$ -Cimbi-36 in this study is also in accordance with preclinical studies; effective dose was found to be 4.9  $\mu\text{Sv}/\text{MBq}$  and 7.7  $\mu\text{Sv}/\text{MBq}$ , when extrapolating from pig and rat dosimetry, respectively [11]. In the case of  $^{11}\text{C}$ -Cimbi-36, studies in pigs thus proved to have a better translational value compared with rats, but differences across species cannot be predicted [13]. The decision of whether to undertake human radiation dosimetry studies of a new radioligand, when  $^{11}\text{C}$ -labeled tracers show this limited variability, should therefore be considered. Dosimetry studies are both costly and time-consuming, and expose healthy individuals to radiation, with (perhaps) no added benefit compared with a conservative

estimate based on the highest reported effective dose, as suggested in one study [13]. A generic model for  $^{11}\text{C}$ -labeled substances for brain imaging predicts an effective dose of 4.5  $\mu\text{Sv}/\text{MBq}$ , based on the assumption that radioactivity is rapidly and uniformly distributed throughout all tissue [24]. Yet, in the absence of preclinical data or model that can predict with sufficient certainty if one organ receives an excessive absorbed dose, it can be justified to conduct a small number of whole-body scans to take this possible scenario into account.

Despite similar radiation dosimetry for the two tracers,  $^{11}\text{C}$ -Cimbi-36 continues to be the preferred radioligand for 5-HT<sub>2A</sub>R neuroimaging studies, as it has a better signal-to-noise ratio in the brain [15].

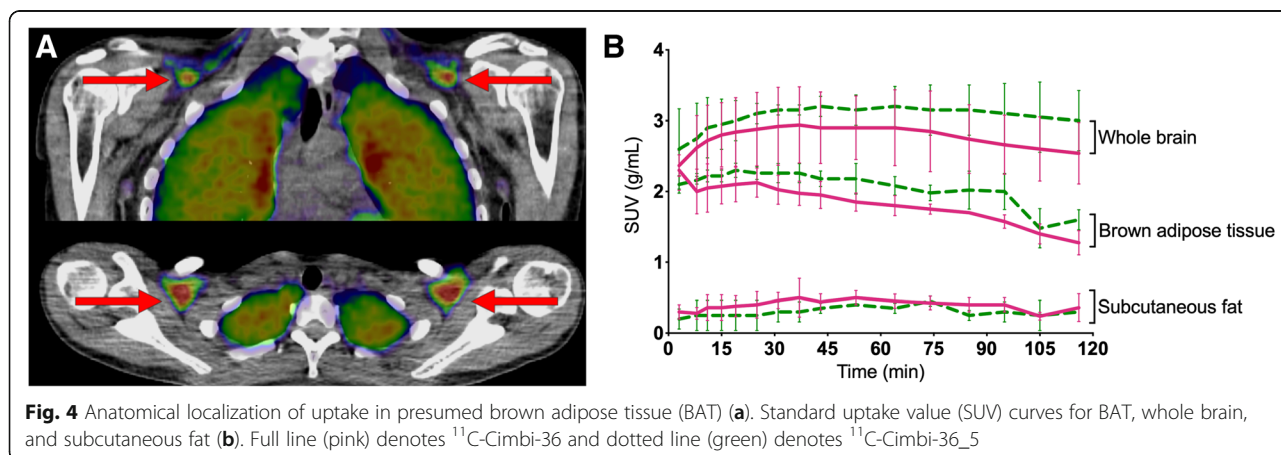
**Biodistribution, pharmacology, and metabolism**

Biodistribution can help shed light on pharmacokinetics [25], but interpretation of the SUV curves for the internal organs should be done with caution, as they



represent both the parent tracers and their radiolabeled metabolites. This leaves the following possible interpretations of radioactivity uptake: 1) specific binding of parent tracer; 2) enzymes or other sites of metabolism of parent tracer or labeled metabolites; 3) excretion of parent tracer or radiometabolites; 4) non-specific binding of parent tracer or radiometabolites. As biodistribution of Cimbi-36 is particularly interesting because of its use as a recreational drug (alias 25B-NBOMe) with many case reports of toxicity and even fatalities [26], we will discuss 1–3 in more detail in the following.

Specific binding: Cimbi-36 not only binds to the 5-HT<sub>2A</sub>R, but also has affinity for, e.g., the 5-HT<sub>2C</sub> receptor and Sigma 2 receptors; however, the affinity for these two receptors are 15- [27] and 120-fold [10] lower, respectively. As no blocking agent was used in the present study, potential 5-HT<sub>2A/C</sub>R binding in extracerebral tissue cannot be determined with complete certainty from our data. The primary focus of 5-HT is on its effects in the central nervous system, but peripheral 5-HT is implicated in many bodily functions, such as energy metabolism through actions in the gut, pancreas, and fatty tissues [28–31] but also immune response,



inflammation [32], and pain stimuli [33]. High uptake in, e.g., the small intestines or the pancreas might thus represent specific 5-HT<sub>2A/2C</sub>R binding. 5-HT<sub>2A</sub>Rs are also found on human alpha, beta, and delta cells in the pancreas [29]. In type 2 diabetic patients, increased expression of the 5-HT<sub>2A</sub>R was found in unspecified pancreatic islet cells relative to healthy controls [34], while 5-HT<sub>2C</sub>R inhibits insulin secretion by beta cells in a diabetic mouse model [35]. These findings may in part explain the hyperglycemia seen in several cases of NBOMe intoxication [7].

Surprisingly, we found high uptake in what we believe to be brown adipose tissue (BAT). A newly conducted study links administration of 25B-NBOMe in rats to hyperthermia and thermogenesis of BAT [36]. These effects are thought to be mediated through peripheral 5-HT<sub>2A</sub>Rs as central adrenergic and serotonergic neurons were selectively destroyed by neurotoxins in these animals. BAT stimulation by 5-HT has been shown to inhibit beta-adrenergic signaling and BAT thermogenesis [29] through the 5-HT<sub>3</sub>R [30, 37], while 5-HT<sub>2A</sub>R stimulation increases BAT thermogenesis [38, 39]. Thus, peripheral 5-HT might have bidirectional physiological effects on BAT thermogenesis, depending on 5-HT receptor expression pattern, which in turn could reflect differences in the physiological state (active vs. inactivated BAT). Interestingly, hyperthermia is a common complication in NBOMe intoxications, with and without seizures [7], and peripheral 5-HT<sub>2A/2C</sub>R effects on BAT might be a contributing factor.

The severe toxicity of 25B-NBOMe and other 5-HT<sub>2</sub>R selective agonists is curious in light of the relatively low toxicity of classical non-selective 5-HT<sub>2A</sub>R hallucinogens such as psilocybin, LSD, and mescaline [40, 41]. Considering the different effects on BAT thermogenesis mediated by different 5-HT receptors, toxicity might then arise because of, rather than despite, high selectivity. Other factors, such as inter-individual differences in metabolism might also contribute, as discussed below.

**Metabolism:** Not surprisingly, the liver showed high uptake beyond the initial perfusion phase reflecting the extensive metabolism of the parent tracers. In both pig and human, the metabolic route is through *O*-demethylation (phase I reaction, Fig. 1), primarily at the 5'-position, followed by glucuronide conjugation (phase II reaction) [14]. <sup>11</sup>C-labeling in the 2-methoxybenzyl-position (<sup>11</sup>C-Cimbi-36) gives rise to two radiometabolite fractions: M1, comprising small polar radiometabolites, which is likely a mixture of <sup>11</sup>C-formaldehyde, <sup>11</sup>C-formic acid, and <sup>11</sup>C-CO<sub>2</sub>/bicarbonate; and M2, which was identified as a <sup>11</sup>C-glucuronide conjugate [14]. Changing the <sup>11</sup>C-labeling to the 5'-methoxy-4-bromophenethylamine position (<sup>11</sup>C-Cimbi-36\_5) eliminates

the radiolabeled form of the glucuronide conjugate (M2), leaving only the M1 fraction [15]. Caspar et al. [42] found that the *O*-demethylation is catalyzed by CYP2C19 (cytochrome P-450 enzyme) and CYP2D6, and the relative contribution to hepatic clearance was estimated to be 69% for CYP2D6, with the remaining clearance attributed to CYP2C19 and CYP3A4 (catalyzing *N*-dealkylation and/or hydroxylation). These CYP isoforms are also found in the small intestines [43], which we hypothesize account for part of the high uptake of <sup>11</sup>C-Cimbi-36 in the proximal small intestine throughout the scan. The other part possibly representing specific binding to 5-HT<sub>2A/2C</sub>Rs. <sup>11</sup>C-Cimbi-36 also shows higher uptake than <sup>11</sup>C-Cimbi-36\_5 in the liver, which we speculate is because the resulting phase I metabolite of the former goes on to being glucuronidated by glucuronosyltransferases (UGT) [44]. The labeled metabolites of <sup>11</sup>C-Cimbi-36\_5 are small polar, likely volatile, substances [15] and therefore not likely retained in the liver to the same degree. The same pattern is seen in the kidneys, in which several UGTs are present [43], although transporters in the renal tubule cells responsible for the secretion of the <sup>11</sup>C-labeled glucuronide conjugate might better explain the difference in uptake seen between the tracers. This is further substantiated as the difference in uptake does not emerge until approximately 20 min into the scan, when most of the activity is in the form of the glucuronide conjugate [15].

Inter-individual differences due to genetic variability in CYP isoforms or induction/inhibition by foods or drugs may contribute to the toxicity of NBOMes. We note that the red and purple lines are near identical in whole blood (Fig. 3) and follow the same shape in the liver, kidney, and bladder. The case is similar for the blue and green lines, which follow a different shape and have higher uptake in the liver, while the orange is somewhat in-between. The liver transit time may thus reflect differences in CYP profiles with regard to metabolic rate or route.

**Excretion:** The two organs with the most pronounced difference in uptake between the two labeling positions were the urinary bladder and the gallbladder, pointing to an unambiguous difference in excretory pathways of the <sup>11</sup>C-labeled metabolites of the two tracers. For the gallbladder, this difference is not reflected in the dosimetry results, as the onset of the difference happens after three half-lives of the radioactive label. It is important to keep in mind that, unlike most of the organs in the human body, the urinary bladder and the gallbladder do not have fixed volumes but expand and contract on physiological demand, and thus the concentrations depend on two independent variables. Emptying by the gallbladder into the small intestines might also contribute to the high uptake in the



proximal small intestines, but then again, these SUVs are relatively stable during the course of the scan. For  $^{11}\text{C}$ -Cimbi-36, the urinary bladder SUV curves (Fig. 2) vary immensely between the subjects as was the case for the absolute amount of excreted substance (Fig. 3d). As the cold doses in our study (ranging 0.25–0.61  $\mu\text{g}$ ) are well below pharmacologically active doses of NBOMes (usually 0.5–1 mg [7]), we cannot exclude the possibility that metabolic route and excretory rate differ in these settings.

To further explore the biodistribution of 5-HT<sub>2A/2C</sub> receptors and metabolism, whole-body scans after pre-treatment with blocking agents such as Ketanserin (5-HT<sub>2A</sub> receptor antagonist) or CYP inhibitors could be performed, and CYP isoform profiling of participants could be correlated.

## Conclusion

The 5-HT<sub>2A</sub> receptor agonist PET radioligand  $^{11}\text{C}$ -Cimbi-36 has a favorable radiation dosimetry profile with an effective dose of 5.5  $\mu\text{Sv}/\text{MBq}$ , which allows for injection of 1.8 GBq per study in healthy volunteers, thus making  $^{11}\text{C}$ -Cimbi-36 eligible for studies involving a series of PET scans in a single subject.

The biodistribution reflects the rapid metabolism and glucuronidation of  $^{11}\text{C}$ -Cimbi-36 in the liver and subsequent excretion of this metabolite through the kidneys and gallbladder, but also shows considerable variability, that might play into the toxicity seen for the unlabeled version, 25B-NBOMe, when used as a recreational drug. Surprisingly, uptake throughout the scan was seen in periclavicular brown adipose tissue for four subjects, quite possibly representing specific 5-HT<sub>2A/2C</sub> receptor binding.

## Additional file

**Additional file 1:** TIAC values. (XLSX 30 kb)

### Abbreviations

5-HT<sub>2A</sub>: Serotonin 2A receptor; AUC: Area under the curve; BAT: Brown adipose tissue; CYP: Cytochrome P-450 enzyme; PET: Positron emission tomography; SUV: Standard uptake value; TAC: Time-activity curve; TIAC: Time-integrated activity coefficient; UGT: Glucuronosyltransferases; VOI: Volume of interest; WB: Whole blood

### Acknowledgements

Technical assistance of Lone Ibsgaard Fryer, Susanne Svalling, Dorte Skovgaard, Gerda Thomsen, Svitlana Olsen and Peter Steen Jensen is greatly acknowledged.

### Authors' contributions

AJ designed study, collected and analyzed the data, drafted the manuscript, and gave approval of the final manuscript. SH designed the study, analyzed the data, revised the manuscript for intellectual content, and gave approval of the final manuscript. BD designed the study, collected the data, revised the manuscript for intellectual content, and gave approval of the final manuscript. SK analyzed the data, revised the manuscript for intellectual

content, and gave approval of the final manuscript. JK conceptualized the study, revised the manuscript for intellectual content, and gave approval of the final manuscript. GK designed and conceptualized the study, revised the manuscript for intellectual content, and gave approval of the final manuscript. HH designed and conceptualized the study, collected and analyzed the data, revised the manuscript for intellectual content, and gave approval of the final manuscript.

### Funding

This study was financially supported by the Lundbeck Foundation, the John and Birthe Meyer Foundation, Aase and Ejnar Danielsens Fond, and Arvid Nilssons Fond.

### Availability of data and materials

Authors can confirm that all relevant data are included in the article and/or its supplementary information files.

### Ethics approval and consent to participate

The study was approved by the Ethics Committee for the Capital Region of Denmark (protocol no. H-15001910) and the Danish Health and Medicine Authority (EudraCT no. 2015-004256-21). The study was registered as a clinical trial (NCT02629003) at [ClinicalTrials.gov](http://ClinicalTrials.gov) and was performed in accordance with the recommendation for Good Clinical Practice.

### Consent for publication

The authors provide consent for publication of this research paper.

### Competing interests

The authors declare that they have no competing interests.

### Author details

<sup>1</sup>Neurobiology Research Unit and Center for Integrated Molecular Brain Imaging, Rigshospitalet, Building 6931, Blegdamsvej 9, DK-2100 Copenhagen, Denmark. <sup>2</sup>Faculty of Health and Medical Sciences, University of Copenhagen, Copenhagen, Denmark. <sup>3</sup>PET and Cyclotron Unit, Rigshospitalet, Copenhagen, Denmark. <sup>4</sup>Department of Drug Design and Pharmacology, Faculty of Health and Medical Sciences, University of Copenhagen, Copenhagen, Denmark.

Received: 12 April 2019 Accepted: 20 June 2019

Published online: 31 July 2019

### References

1. Ettrup A, da Cunha-Bang S, McMahon B, Lehel S, Dyssegaard A, Jørgensen LM, et al. Serotonin 2A receptor agonist binding in the human brain with [ $^{11}\text{C}$ ]Cimbi-36. *J Cereb Blood Flow Metab.* 2014;34:1188–96.
2. Beliveau V, Ganz M, Feng L, Ozenne B, Højgaard L, Fisher PM, et al. A high-resolution in vivo atlas of the human brain's serotonin system. *J Neurosci.* 2017;37:120–8.
3. Frokjaer VG, Mortensen EL, Nielsen FÅ, Haugbol S, Pinborg LH, Adams KH, et al. Frontolimbic serotonin 2A receptor binding in healthy subjects is associated with personality risk factors for affective disorder. *Biol Psychiatry.* 2008;63:569–76.
4. Bhagwagar Z, Hinz R, Taylor M, Fancy S, Cowen P, Grasby P. Increased 5-HT 2A receptor binding in euthymic, medication-free patients recovered from depression: a positron emission study with [ $^{11}\text{C}$ ]MDL 100,907. *Am J Psychiatry.* 2006;163:1580–7.
5. Sullivan LC, Clarke WP, Berg KA. Atypical antipsychotics and inverse agonism at 5-HT<sub>2</sub> receptors. *Curr Pharm Des.* 2015;21:3732–8.
6. Madsen MK, Fisher PM, Burmester D, Dyssegaard A, Stenbæk DS, Kristiansen S, et al. Psychedelic effects of psilocybin correlate with serotonin 2A receptor occupancy and plasma psilocin levels. *Neuropsychopharmacology.* 2019;44:1328–34.
7. Halberstadt AL. Pharmacology and toxicology of N-benzylphenethylamine ("NBOMe") hallucinogens. *Curr Top Behav Neurosci.* 2017;32:283–311.
8. Shalgunov V, van Waarde A, Booij J, Michel MC, Dierckx RAJO, Elsinga PH. Hunting for the high-affinity state of G-protein-coupled receptors with agonist tracers: theoretical and practical considerations for positron emission tomography imaging. *Med Res Rev.* 2019;39:1014–52.

9. Gandhimathi A, Sowdhamini R. Molecular modelling of human 5-hydroxytryptamine receptor (5-HT<sub>2A</sub>) and virtual screening studies towards the identification of agonist and antagonist molecules. *J Biomol Struct Dyn*. 2016;34(5):952–70.
10. Ettrup A, Hansen M, Santini MA, Paine J, Gillings N, Palner M, et al. Radiosynthesis and in vivo evaluation of a series of substituted <sup>11</sup>C-phenethylamines as 5-HT<sub>2A</sub> agonist PET tracers. *Eur J Nucl Med Mol Imaging*. 2011;38:681–93.
11. Ettrup A, Holm S, Hansen M, Wasim M, Santini MA, Palner M, et al. Preclinical safety assessment of the 5-HT<sub>2A</sub> receptor agonist PET radioligand [<sup>11</sup>C]Cimbi-36. *Mol Imaging Biol*. 2013;15:376–83.
12. Finnema SJ, Stepanov V, Ettrup A, Nakao R, Armini N, Svedberg M, et al. Characterization of [<sup>11</sup>C]Cimbi-36 as an agonist PET radioligand for the 5-HT<sub>2A</sub> and 5-HT<sub>2C</sub> receptors in the nonhuman primate brain. *Neuroimage*. 2014;84:342–53.
13. Zanotti-Fregonara P, Lammertsma AA, Innis RB. Suggested pathway to assess radiation safety of <sup>11</sup>C-labeled PET tracers for first-in-human studies. *Eur J Nucl Med Mol Imaging*. 2012;39:544–7.
14. Leth-Petersen S, Gabel-Jensen C, Gillings N, Lehel S, Hansen HD, Knudsen GM, et al. Metabolic fate of hallucinogenic NBOMes. *Chem Res Toxicol*. 2016;29:96–100.
15. Johansen A, Hansen HD, Svarer C, Lehel S, Leth-Petersen S, Kristensen JL, et al. The importance of small polar radiometabolites in molecular neuroimaging: A PET study with [<sup>11</sup>C]Cimbi-36 labeled in two positions. *J Cereb Blood Flow Metab*. 2018;38:659–68.
16. Persson M, Skovgaard D, Brandt-Larsen M, Christensen C, Madsen J, Nielsen CH, et al. First-in-human uPAR PET: Imaging of cancer aggressiveness. *Theranostics*. 2015;5:1303–16.
17. Skovgaard D, Persson M, Brandt-Larsen M, Christensen C, Madsen J, Klausen TL, et al. Safety, dosimetry, and tumor detection ability of <sup>68</sup>Ga-NOTA-AE105: first-in-human study of a novel radioligand for uPAR PET imaging. *J Nucl Med*. 2016;58:379–86.
18. Stabin MG, Siegel JA. Physical models and dose factors for use in internal dose assessment. *Health Phys*. 2003;85:294–310.
19. ICRP Publication. The 2007 Recommendations of the International Commission on Radiological Protection. ICRP publication 103. *Ann ICRP*. 2007;37:1–332.
20. Stabin MG. Fundamentals of nuclear medicine dosimetry. New York: Springer; 2008.
21. Leitner BP, Huang S, Brychta RJ, Duckworth CJ, Baskin AS, McGehee S, et al. Mapping of human brown adipose tissue in lean and obese young men. *Proc Natl Acad Sci*. 2017;114:8649–54.
22. ICRP. Radiological Protection in Biomedical Research. ICRP Publication 62. *Ann ICRP*. 1992;22(3).
23. Van Der Aart J, Hallett WA, Rabiner EA, Passchier J, Comley RA. Radiation dose estimates for carbon-11-labelled PET tracers. *Nucl Med Biol*. 2012;39:305–14.
24. Nosslin B, Johansson L, Leide-Svegborn S, Liniecki J, Mattsson S, Taylor DM. A generic model for <sup>11</sup>C labelled radiopharmaceuticals for imaging receptors in the human brain. *Radiat Prot Dosimetry*. 2003;105:587–91.
25. Heller AA, Lockwood SY, Janes TM, Spence DM. Technologies for measuring pharmacokinetic profiles. *Annu Rev Anal Chem*. 2018;11:79–100.
26. Suzuki J, Dekker MA, Valenti ES, Arbello Cruz FA, Correa AM, Poklis JL, et al. Toxicities associated with NBOMe ingestion—a novel class of potent hallucinogens: a review of the literature. *Psychosomatics*. 2015;56:129–39.
27. Herth MM, Petersen IN, Hansen HD, Hansen M, Ettrup A, Jensen AA, et al. Synthesis and evaluation of <sup>18</sup>F-labeled 5-HT<sub>2A</sub> receptor agonists as PET ligands. *Nucl Med Biol*. 2016;43:455–62.
28. Banskota S, Ghia JE, Khan WI. Serotonin in the gut: blessing or a curse. *Biochimie*. 2019;161:56–64.
29. El-Merahbi R, Löffler M, Mayer A, Sumara G. The roles of peripheral serotonin in metabolic homeostasis. *FEBS Lett*. 2015;589:1728–34.
30. Oh CM, Park S, Kim H. Serotonin as a new therapeutic target for diabetes mellitus and obesity. *Diabetes Metab J*. 2016;40:89–98.
31. Kim H, Toyofuku Y, Lynn FC, Chak E, Uchida T, Mizukami H, et al. Serotonin regulates pancreatic beta cell mass during pregnancy. *Nat Med*. 2010;16:804–8.
32. Shajib MS, Khan WI. The role of serotonin and its receptors in activation of immune responses and inflammation. *Acta Physiol*. 2015;213:561–74.
33. Sommer C. Serotonin in pain and analgesia: actions in the periphery. *Mol Neurobiol*. 2004;30:117–25.
34. Bennet H, Balhuizen A, Medina A, Dekker Nitert M, Ottosson Laakso E, Essén S, et al. Altered serotonin (5-HT) 1D and 2A receptor expression may contribute to defective insulin and glucagon secretion in human type 2 diabetes. *Peptides*. 2015;71:113–20.
35. Zhang Q, Zhu Y, Zhou W, Gao L, Yuan L, Han X. Serotonin receptor 2C and insulin secretion. *PLoS One*. 2013;8:e54250.
36. Nakamura M, Shintani-Ishida K, Ikegaya H. 5-HT<sub>2A</sub> receptor agonist-induced hyperthermia is induced via vasoconstriction by peripheral 5-HT<sub>2A</sub> receptors and brown adipose tissue thermogenesis by peripheral serotonin loss at a high ambient temperature. *J Pharmacol Exp Ther*. 2018;367:356–62.
37. Oh CM, Namkung J, Go Y, Shong KE, Kim K, Kim H, et al. Regulation of systemic energy homeostasis by serotonin in adipose tissues. *Nat Commun*. 2015;6:1–12.
38. Ootsuka Y, Blessing WW. Thermogenesis in brown adipose tissue: Increase by 5-HT<sub>2A</sub> receptor activation and decrease by 5-HT<sub>1A</sub> receptor activation in conscious rats. *Neurosci Lett*. 2006;395:170–4.
39. Ootsuka Y, Blessing WW, Nalivaiko E. Selective blockade of 5-HT<sub>2A</sub> receptors attenuates the increased temperature response in brown adipose tissue to restraint stress in rats. *Stress*. 2008;11:125–33.
40. Studerus E, Komater M, Hasler F, Vollenweider FX. Acute, subacute and long-term subjective effects of psilocybin in healthy humans: a pooled analysis of experimental studies. *J Psychopharmacol*. 2011;25:1434–52.
41. Krebs TS, Johansen PØ. Psychedelics and mental health: a population study. *PLoS One*. 2013;8:1–9.
42. Caspar AT, Meyer MR, Maurer HH. Human cytochrome P450 kinetic studies on six N-2-methoxybenzyl (NBOMe)-derived new psychoactive substances using the substrate depletion approach. *Toxicol Lett*. 2018;285:1–8.
43. Uhlen M, Berling H, von Feilitzen K, Nielsen J, Szgyarto CA-K, Edlund K, et al. Tissue-based map of the human proteome. *Science*. 2015;347:1260419.
44. Boumrah Y, Humbert L, Phanithavong M, Khimeche K, Dahmani A, Allorge D. In vitro characterization of potential CYP- and UGT-derived metabolites of the psychoactive drug 25B-NBOMe using LC-high resolution MS. *Drug Test Anal*. 2016;8:248–56.

## Publisher's Note

Springer Nature remains neutral with regard to jurisdictional claims in published maps and institutional affiliations.

**Submit your manuscript to a SpringerOpen<sup>®</sup> journal and benefit from:**

- Convenient online submission
- Rigorous peer review
- Open access: articles freely available online
- High visibility within the field
- Retaining the copyright to your article

---

Submit your next manuscript at ► [springeropen.com](https://www.springeropen.com)